Journal of Power Sources 270 (2014) 79–91

Contents lists available at ScienceDirect

Journal of Power Sources

journal homepage: www.elsevier.com/locate/jpowsour

Effect of redox treatments on $Ce_{0.50}Zr_{0.50}O_2$ based solid oxide fuel cell anodes

Marta Boaro [a, *], Alfonsina Pappacena [a], Chiara Abate [a], Matteo Ferluga [a], Jordi Llorca [b], Alessandro Trovarelli [a]

[a] Dipartimento di Chimica, Fisica e Ambiente, via Cotonificio 108, Università di Udine, Udine 33100, Italy
[b] Institut de Tècniques Energètiques and Centre for Research in Nanoengineering, Universitat Politècnica de Catalunya, Barcelona 08028, Spain

HIGHLIGHTS

- SOFC anode of Cu–$Ce_{0.50}Zr_{0.50}O_2$/YSZ were prepared by infiltration.
- $Ce_{0.50}Zr_{0.50}O_2$ redox properties and cell performances were correlated.
- TPR measurements are an useful tool to study interactions in the anode components.
- Redox cycles at 973 K can help activation and stabilization of anode performance.
- Electrodes properties are controlled by Copper and $Ce_{0.50}Zr_{0.50}O_2$ interplay.

GRAPHICAL ABSTRACT

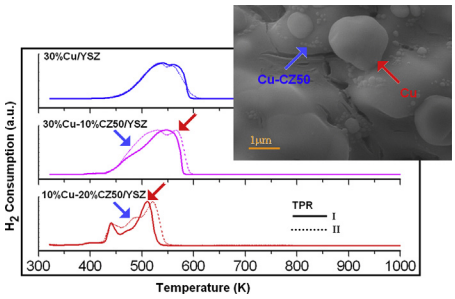

ARTICLE INFO

Article history:
Received 22 March 2014
Received in revised form
13 June 2014
Accepted 11 July 2014
Available online 21 July 2014

Keywords:
SOFC
Redox tolerance
Ceria–zirconia
Pyrochlore phase
Copper anode

ABSTRACT

This work investigates the activity of copper modified $Ce_{0.50}Zr_{0.50}O_2$ (Cu–CZ) based anodes prepared through subsequent impregnation steps into a porous YSZ matrix. The ceria–zirconia oxide was reduced at increasing temperatures and the effect of structural changes on anode performance investigated at 973 K under humidified H_2. Performance of all cells increased after one redox cycle due to a decrease of both the anode polarization and the ohmic resistance of the cell. The redox behaviour of Cu–CZ anode was investigated in a symmetrical cell configuration and it was observed that subsequent redox cycles lead to an activation and stabilization of the electrodes. SEM and EIS characterizations showed that this is mainly attributable to a rearrangement of the morphology and microstructure of the CZ oxide at the electrode/electrolyte interface and to an improvement of copper distribution into the porous electrode matrix. It is inferred that the interplay of copper and CZ favours the promotion of anode activity by increasing the number of active sites; moreover it stabilizes the redox behaviour of the electrode. An optimization of electrical and structural properties of Cu–CZ composites was also discussed.

1. Introduction

Solid oxide fuel cells (SOFCs) have a high intrinsic efficiency for interconversion between chemical and electrical energy, fuel flexibility, which is unmatched by other fuel cell technologies and easy modularity. Therefore, SOFCs may constitute a strategic technology to favour the transition from a "carbon dirty economy", based on the use of fossil fuels, to a "green economy" based on the use of renewable sources and distributed energy generation [1]. However, in order to increase the competitiveness of SOFC technology in the sector of distributed energy generation, cogeneration

* Corresponding author.
E-mail addresses: marta.boaro@uniud.it, mboaro2000@yahoo.it (M. Boaro).

http://dx.doi.org/10.1016/j.jpowsour.2014.07.069
0378-7753/

and portable applications, it is necessary to develop systems able to operate at lower temperatures (500–700 °C) with different types of fuels and in variable operating conditions [2–4]. In recent years, a lot of progress has been made in the field of new materials [5,6], and new manufacturing concepts, such as metal supported cells [7], impregnated electrodes [8,9], and micro cells have been developed to achieve these goals [10].

In the development of SOFC anode materials, Nickel–Yittria stabilized Zirconia (Ni–YSZ) cermet is still the most used anode and numerous efforts have been spent on overcoming its durability issues related to a poor tolerance to sulphur, a high activity to catalyse carbon formation and to a scarce redox resistance caused by metal coarsening [11,12].

The different strategies adopted to achieve the development of more durable and active anodes are summarized in several reviews [13–16]. In particular, attention has been focused on the optimization of anodes containing a good oxidation catalyst, such as ceria [17–19], and on the use of other transition metals and alloys [20–23].

The advantages of introducing CeO_2 as composite materials and/or as separated layers in SOFC anodes are linked to the very high catalytic activity of ceria based materials towards hydrocarbon oxidation. In addition, these materials possess substantial mixed ionic and n-type electronic conductivity which contributes to the extension of the three phase boundary to a wide portion of the anode surface. On the other hand, these materials have low electronic conductivity and could suffer from dimensional instability due to the redox properties of cerium ions, when exposed to a large $p(O_2)$ variation [16]. Oxygen transport properties and the reducibility of ceria can be enhanced by acceptor type doping [24–26], however these doped oxides, usually show lower catalytic activity for hydrocarbon oxidation [27].

Concerning the endurance to carbon formation and redox tolerance, encouraging results were achieved with anodes made by infiltration of Cu and CeO_2 into a YSZ porous matrix. Per contra, this type of electrode suffers from thermal stability issues due to sintering of both copper and ceria [16,28–30]. Moreover, when fed with heavier hydrocarbons Cu–CeO_2/YSZ anodes still need an adequate ratio of steam/fuel to prevent tar accumulation caused by gas-phase pyrolysis reactions [31,32].

A successful attempt to improve the thermal stability and carbon tolerance of this type of electrodes was achieved by substituting pure ceria with ceria–zirconia solid solutions [33–35]. It is indeed well known that the introduction of Zr^{4+} in the crystal lattice of CeO_2 increases the reducibility and the oxygen storage capacity, as well as the thermal stability and the electrical conductivity of the fluorite structure [36–40]. The structural and redox properties of ceria zirconia solid solutions depend on their composition, and they are profoundly affected by the method of synthesis [41,42] as well as by the redox and/or thermal treatments undergone [43–46]. These properties have been thoroughly investigated in the development of advanced ceria based catalysts for environmental and industrial applications [47,48]. Conversely, only a few studies report the use of these materials as anode active catalysts [49–54], and to our knowledge there are no specific studies about the effects of their redox properties on cell performance.

In order to gain insight into this aspect, we preliminarily investigated structural, redox and electrical properties of solid solutions with different Ce/Zr ratio in form of dense pellets, before and after redox treatments [55]. Alternated reduction and oxidation steps, respectively at 1273 K and 873 K, promoted the reduction at a lower temperature in all samples investigated, with promotion strongly related to ceria loading. The same rank was observed for the electrical conductivity of these materials; however, an enhancement of electrical conductivity after the redox treatments was observed only for the $Ce_{0.50}Zr_{0.50}O_2$ composition. In this case the increase in conductivity by an order of magnitude was linked to the significant structural changes occurring in the reduction–oxidation cycle [55]. According to these results, both $Ce_{0.80}Zr_{0.20}O_2$ and $Ce_{0.50}Zr_{0.50}O_2$ are interesting compositions to be investigated as anode components, the former for its higher conductivity and reducibility, the latter for its peculiar redox properties. Recent studies on the electrochemical properties of ceria–zirconia oxides have confirmed the superior activity of cerium rich compositions in the development of SOFC anodes, especially when carbon and renewable fuels are used [34,35,49–54].

In this study we focused on the effects of redox properties of $Ce_{0.50}Zr_{0.50}O_2$ (CZ) on the performance of Cu–$Ce_{0.50}Zr_{0.50}O_2$ (Cu–CZ) based anode prepared by infiltration of the active components into a YSZ porous layer. In fact, the CZ structure presents peculiar redox behaviour since its cation and anion sub lattices can be modified with appropriate reduction, obtaining either cubic or tetragonal metastable phases characterized by a higher reducibility and increased electronic conductivity [55]. In order to evaluate if the formation of these enhanced phases under SOFC operating conditions could contribute to improve the anode performance, the study was conducted in different steps. First, we focused on investigating the effect of reduction at increasingly temperature, on the CZ catalyst infiltrated into a YSZ porous layer. The structural and morphological changes induced by the reduction on CZ infiltrated catalysts were investigated through a parallel study on CZ powders that underwent the same treatments. Once ascertained the formation of different CZ50 phases for the infiltrated catalysts, we compare the electrochemical activity of the corresponding Cu–CZ/YSZ anodes, evaluating polarization curves and electrochemical impedance spectra of specifically designed cells. As a final step, we evaluated the effect of oxidation and reduction cycles at the cell operating temperature on these Cu–CZ/YSZ electrodes. The main aim of the whole study was to discriminate between the different contributions that would lead to redox tolerant anodes based on this Ce/Zr composition.

2. Experimental section

2.1. Catalysts synthesis

CZ solid solution was prepared by a modified solution-combustion citrate synthesis [56]. $Ce(NO_3)_3{}^*6H_2O$ (Treibacher) and $ZrO(NO_3)_2{}^*5H_2O$ (Sigma–Aldrich) were separately dissolved in distilled water and then mixed together to obtain a 1:1 Ce:Zr cation ratio; citric acid (CA) was then added to the solutions in molar concentration equal to that of metal ions. To improve complexation, the solution was heated at 343 K and kept under stirring for 1 h. Part of the solution was ignited in air to 773 K at 10 K min^{-1} to obtain the mixed oxide powder for further treatments and characterizations, and the rest of the solution was used to infiltrate the oxide in the cell anodic layer.

$La_{0.8}Sr_{0.2}MnO_3$ (LSM) was prepared through a modified Pechini synthesis [57] using a ratio between citric acid (CA) and ethylene glycol (EC) equal to one and a ratio of five between CA and the total cation moles. The nitrate precursors were dissolved in the desired stoichiometric ratio with a minimum amount of water, the solution was mixed to a CA and EC solution to obtain a total volume of 100 ml. The solution was left to gel under stirring at 353 K and then calcined at 1073 K for 2 h and characterized.

2.2. Cells and electrodes manufacturing

Symmetrical cells (Cu/YSZ||YSZ||Cu/YSZ; Cu–CZ/YSZ||YSZ||YSZ/CZ–Cu) and button cells (Cu–CZ/YSZ||YSZ||LSM/YSZ) were

prepared by tape-casting method. They consisted of a YSZ wafer that had a dense layer between two porous layers.

The green tapes were prepared as described in Refs. [58], by dispersing YSZ powder (Tosoh Corp.; 8 mol% Y_2O_3-doped ZrO_2) in distilled water with a dispersant (Duramax, D3005, Rohm & Haas) and binders (Duramax B 1000 and Primal HA-12, Rohm and Haas). The porosity was introduced by the addition of graphite (Alfa Aeser, 325 mesh, conductivity grade) and polymethylmethacrylate (PMMA) powder (Porlat K85, Zschimmer & Schwarz) into the green tape. The porosity of the YSZ porous layers were measured by Hg intrusion porosimetry; the results indicated a porosity of 65%.

The button cells were obtained by laminating a porous and a dense layer together by tape casting and cutting regular discs. To obtain the cathode side, a smaller disc of a porous YSZ green layer was attached on the electrolyte side of the green bilayer discs before sintering.

The symmetrical cells were assembled from separately cast porous and electrolyte tapes using a thin layer of the electrolyte slurry as glue aid. Care was taken to align the porous electrodes on opposite side of the electrolyte in order to avoid artefacts in the EIS measurements. Such assembled cells were fired at 873 K for 1 h and 1773 K for 4 h with a sintering ramp of 2 K min^{-1}.

The size and thickness of the three YSZ layers depends on the type of cell. Typically, in the symmetrical cell the dense layer was 280–300 μm thick and the porous layers, 250 μm thick, with a diameter of 18.3 mm and 15 mm respectively. Instead, the button cells had a diameter of 13 mm and a 90–100 μm thick dense electrolyte layer, the anode layer was 280 μm while the cathode layer was 30 μm thick with a diameter of 9 mm. A general view of the cross section of the cells investigated is shown in Fig. 1.

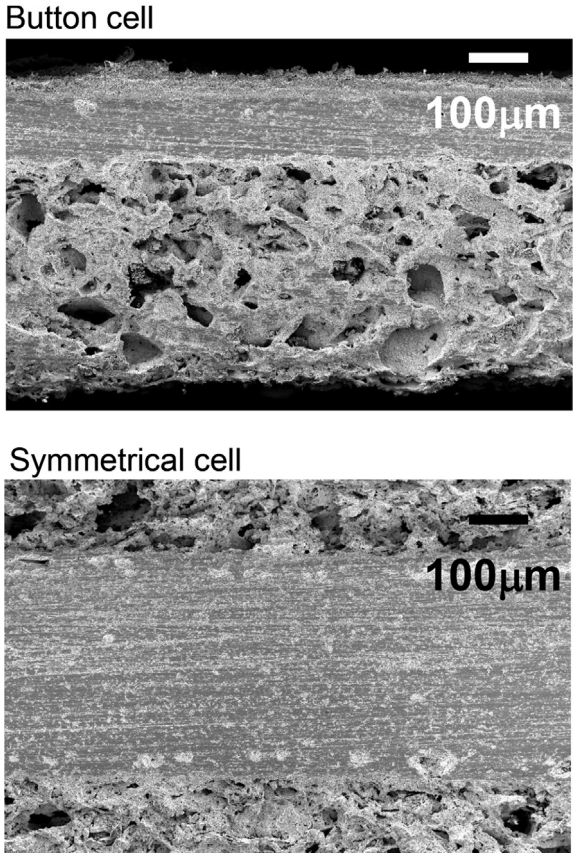

Fig. 1. SEM micrographs of type of cells investigated.

The cathodes of the button cells were prepared by impregnation. After cell sintering, the LSM was infiltrated into the porous cathode layer in the amount of 40 wt%, as suggested in literature [9]; each subsequent impregnation was followed by a calcination step at 773 K, finally the cathode was calcined at 1073 K for 4 h. In order to preserve the LSM integrity, its impregnation was subsequent to that of anode with CZ (10 wt%) and its redox treatment.

The anodes of button cells was multistep impregnated with citrate–nitrate solution of CZ up to a loading of 10 wt%, with calcinations at 773 K for 30 min in between two successive steps; the last step was followed by a calcination at 1073 K. The anode treatments were chosen according to previous studies in order to induce structural changes in the infiltrated CZ [55,59]. Therefore, they were reduced at 1073 K for 72 h, to form a t'-meta-like phase and at 1273 K for 12 h to form a κ-phase with a partial cation ordering. CZ catalysts infiltrated into a slab of YSZ will be indicated as CZ1073o/YSZ (a′), CZ1073r/YSZ (b′), CZ1273r/YSZ (c′), respectively if untreated (i.e. calcined at 1073 K), reduced at 1073 K or at 1273 K. The oxidation step consisted of a 1 K ramp under 1%O_2 in He flow (30 cc min^{-1}), with isotherms at 623 K for 5 h and at 873 K for 2 h. This procedure was adopted to attenuate the mechanical strains induced by the re-oxidation process [59]. The anode preparation was terminated with the copper infiltration using a nitrate solution (30 wt% Cu to the total anode weight) and a final calcination at 973 K.

From YSZ porous green layers, porous pellets (Ø 0.5 cm; 5 mm thick) were also made and impregnated with suitable percentage of CZ (10 or 20 wt%), Cu (30 wt%) or a mixture of the two (CZ 10–20 wt %; Cu 10–30 wt%), this in order to further characterize morphology, and redox behaviour of the anode layers. When necessary, in the text, the composition of electrodes and pellets is indicated as *y*Cu–*x*CZ/YSZ where *y* and *x* are the weight percentage of Cu and CZ respectively in the anode.

In order to provide a rapid view of the different forms of samples considered in this studies, a flowchart diagram of the methods of preparation of catalysts, pellets and fuel cells investigated is given in Schemes 1 and 2.

2.3. Characterization of powders and electrodes

Small amounts of CZ catalyst in form of powder were reduced/oxidized with the same treatments described in the above paragraph for the CZ/YSZ pellets. They will be indicated as CZ1073o (a), CZ1073r (b), CZ1273r (c) if untreated, reduced at 1073 K or at 1273 K respectively. The crystal structures of CZ powders were determined via X-ray powder diffraction technique (XRD) using a Philips PW3040/60 X'pert PRO instrument (equipped with an X'celerator detector) operating at 40 KV and 40 mA, with Ni-filtered CuKα radiation. Diffraction profiles were collected in the 2θ range of 20–140° with a step of 0.02 and a counting time of 40 s/step.

Further structural details of the CZ powders were obtained from Raman spectroscopy. Spectra were collected in the anti-Stokes range of 100–2000 cm^{-1} using Renishaw 1000 spectrometer equipped with Ar ion laser source (excitation wavelength 514 nm, 25 mW).

The measurement of the surface area of the CZ powders and of YSZ pellets before and after impregnation was carried out with a conventional porosity analyser (Tristar 3000, Micromeritics) using the Brunauer–Emmett–Teller (BET) technique (nitrogen adsorption/desorption isotherms at 77 K). The samples were degassed at 150 °C for 2 h to remove physisorbed gases prior to the measurement. To get accurate BET results, the measures were repeated three times and the pellets were in number of five. The SA of the bare pellets was below the lower measurable limit of 0.5 m^2 g^{-1}. The increment of surface area measured after infiltration was

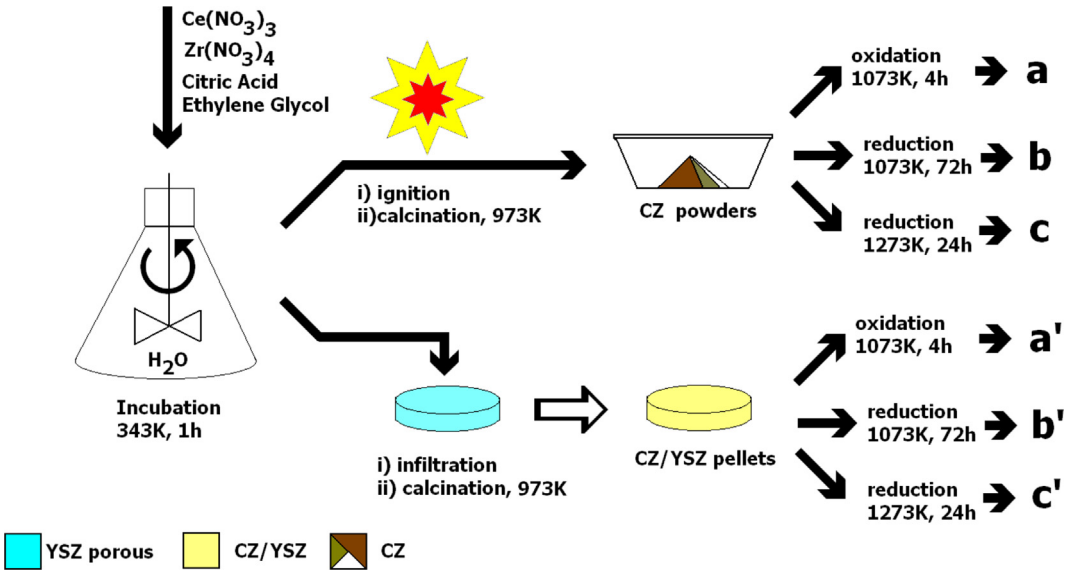

Scheme 1. Preparation of powders and pellets.

therefore attributed to the catalyst by normalizing the value of measured SA for the total mass of the infiltrated catalysts considering almost negligible the contribution of the porous support. An error of 10% is estimated, mainly due to the error in the infiltrated mass value.

High resolution transmission electron microscopy (HRTEM) was performed with a JEOL 2010F microscope equipped with a field emission gun. The point-to-point resolution of the instrument was 0.19 nm and the resolution between lines was 0.14 nm. Samples were deposited from alcohol suspensions over grids with holey-

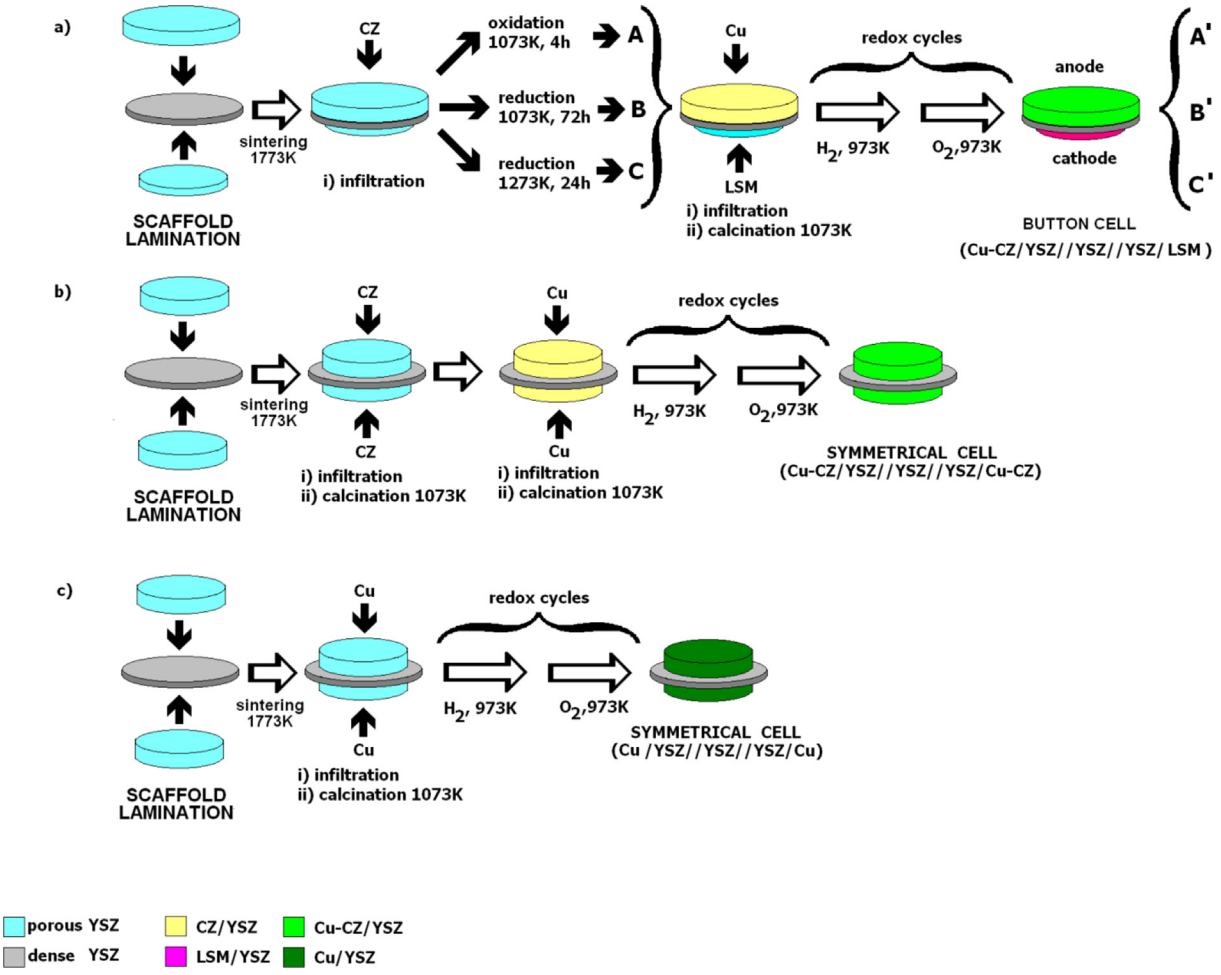

Scheme 2. Preparation of cells.

carbon film. Scanning electron microscopy (SEM) was carried out at 5 kV using a Neon40 Crossbeam Station (Zeiss) equipped with a field emission gun, an energy-dispersive X-ray detector (EDX) or at 20 kV with a EVO-40 XPP (Zeiss) microscopy.

SEM images refer to an anode composition of 20 wt% CZ and 10 wt% Cu despite the tested cell having a composition of 10 wt% CZ and 30 wt% Cu. This alternative composition was chosen since a large amount of copper into the YSZ matrix would have hindered a clear observation of the Cu–CZ interface.

The redox properties of CZ powders and infiltrated pellets have been investigated by temperature programmed reduction (TPR) in a Micromeritics apparatus (Autochem II 2990), using a 4% H_2 in Ar flow (35 STP cc min^{-1}) with a heating ramp of 5 K min^{-1} up to 1073 K, a dwelling time of 30 min and then a 10 K min^{-1} cooling ramp under the same reducing atmosphere. All the samples were pre-treated at 623 K in air in order to remove adsorbed carbonates and water. The anode redox behaviour was also studied with two subsequent TPR measures spaced out by a 2 h oxidation at 973 K.

2.4. Cell testing

For testing, the button cells were attached to an alumina tube with a ceramic adhesive (Aremco, Ceramabond 552). The curing was obtained following a defined heating ramp up to 973 K, under nitrogen flow. The measurements related to the symmetrical cells were carried out in an FC testing system (Material Mates, Company) doted of compensating Kelvin probes.

I–V polarization curves and impedance spectra were obtained using an Amel 7050 potentiostat and an Amel 7200 frequency response analyser with a voltage amplitude of 50 mV and a frequency range spanning from 0.5 Hz to 1 MHz. The operating conditions were 3% humidified H_2 flow (50 cc min^{-1}) at 973 K. The measures were taken after open circuit voltage (OCV) stabilization. The redox cycle was performed the day after the testing cell and it consisted in: 30 min purging step in N_2, 1 h oxidation step in 2%O_2/He, followed by 30 min purging step in N_2 and 1 h reduction step, all steps at 973 K. The performance calculations are made on basis of the cathode area (0.63 cm^2).

It is worth to point out that in this study neither the anode morphology, neither the anode/electrolyte interface were optimized in order to obtain high performance; we focused rather on comparing the investigated materials under operating SOFC conditions. The comparison between different materials was carried out among cells from the same green tape and the results shown are selected in order to be representative of averaged performances.

3. Results and discussion

3.1. Structural and morphological characterization of CZ catalyst powders and CZ/YSZ electrodes

CZ powders and infiltrated CZ electrodes were prepared as described in experimental section, and both powders and infiltrated catalysts underwent redox cycles accordingly to our previous study [55]. Table 1 summarizes the type of treatments. The structural changes induced by these treatments were investigated in the CZ catalysts in form of powder by means of X-ray diffraction and Raman spectroscopy.

The XRD profiles (Fig. 2) show the formation of an apparently cubic phase, when the samples are oxidized (a) or reduced at 1073 K (b) and the formation of a κ-phase after reduction at 1273 K (c) [60]. Despite XRD profiles of samples (a) and (b) being identical, Raman spectra (Fig. 3) reveal significant differences between the two materials. The profile of the sample oxidized at 1073 K (a) shows typical peaks of a tetragonal t′structure [61] while the profile of the other sample shows a broadening of the main peaks (i.e. at 456 cm^{-1}) and the appearance of one peak at 517 cm^{-1} and the onset of a growing peak at 590 cm^{-1}. This indicates that the original symmetry of the t′ phase is lost upon reduction [62] and a new phase is being formed, even if it is difficult to fully define the new structure. The most probable interpretation is represented by the coexistence of tetragonal and pseudo-pyrochlore phases. The spectrum of (c) sample shows peaks at 267 cm^{-1}, 430 cm^{-1}, 590 cm^{-1}, identifying an ordered κ cubic phase [60]. Therefore, with increasingly reduction temperatures, CZ powders progressively form structure with a κ phase symmetry as already demonstrated for dense CZ pellets [55].

Table 1
Morphological and redox properties of CZ powders and infiltrated CZ catalysts.

Samples	Labels	Treatments	Degree of reduction (%)	Surface area (m^2 g^{-1})
CZ1073o		Calc 1073 K, 4 h	54	19
CZ1073r	b	Red 1073 K, 72 h, ox[a]	77	10
CZ1273r	c	Red 1273 K, 24 h, ox[a]	92	4
CZ1073o/YSZ	a′	Calc 1073 K, 4 h	57	14
CZ1073r/YSZ	b′	Red 1073 K, 72 h, ox[a]	71	12
CZ1273r/YSZ	c′	Red 1273 K, 24 h, ox[a]	84	7

[a] Oxidation in two steps: at 623 K, 5 h and at 873 for 2 h [55].

It is well known that high temperature reduction ($T \geq 1273$ K) and mild temperature oxidation ($\leq$873 K) cycles lead to a promotion of ceria zirconia oxide reducibility at lower temperature; this peculiar behaviour is associated with the appearance of pyrochlore phases even if a complete transformation is not necessary [44,45,63]. Therefore, the shape of TPR profiles (Fig. 4) can be taken as an indication of the transformations undergone by the CZ oxides. The TPR profiles of the powders (Fig. 4a) show the growth of a low temperature component as the reduction temperature increases. This is consistent with the structural changes undergone by the powder during their redox treatment. A similar trend is also displayed by the

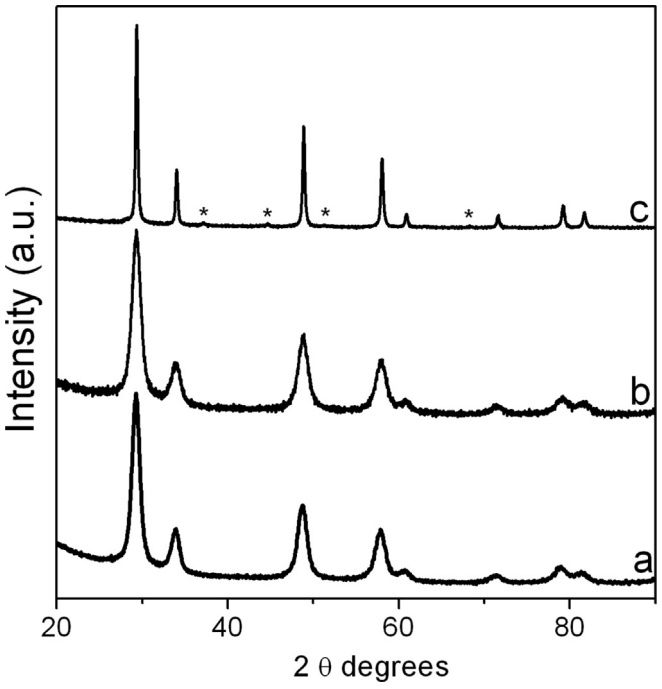

Fig. 2. XRD of CZ powders: (a) CZ1073o; (b) CZ1073r; (c) CZ1273r, * pyrochlore phase.

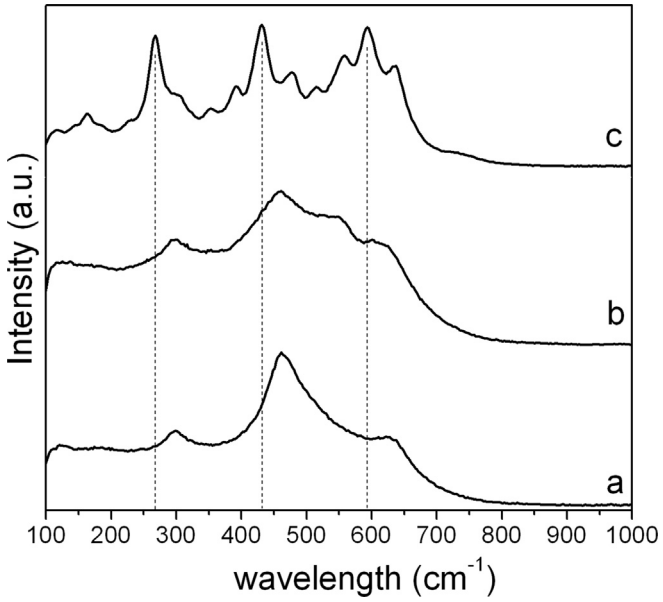

Fig. 3. Raman spectra of CZ powders: (a) CZ1073o; (b) CZ1073r; (c) CZ1273r.

impregnated samples (a′, b′, and c′) (Fig. 4b) even if the relative ratio between the peaks is different. Table 1 reports the corresponding quantitative analysis for the powders and for impregnated pellets and it proves that in both case the reducibility of the samples follows the same rank: CZ1273r > CZ1073r > CZ1073o.

Analogies were also found when considering the specific surface area (SA) of the samples (see Table 1). Unsupported and supported catalysts show a surface area of around 15 $m^2\ g^{-1}$ when reduced at 1073 K, a figure which drops significantly when the temperature of reduction increases. This in line with the fact that the sintering of CeO_2 is accelerated under reducing atmosphere due to the formation of bulk oxygen vacancies in the lattice of the solid, that in turn favours the ion mobility and thus the sintering process [30]. The presence of the support does not seem to hinder the process of coarsening.

The XRD and Raman analyses (not shown) of impregnated materials in the porous YSZ pellets give limited structural information because of a significant loss of sensitivity in presence of the porous substrate. This is due to the small amount of CZ used for the impregnation and also to the overlapping of some identifying peaks with those of the porous substrate. Although it was not possible to observe experimentally the structural evolution of infiltrated powders, similarities between morphological and redox properties of supported and unsupported oxides were evidenced when identical treatments were involved. This entails that the impregnated oxides underwent the same structural changes occurring in the unsupported ones. In addition, under our experimental conditions, the porous matrix seemed to have the sole effect of speeding up the structural transformation. The increased effectiveness of the treatment in the former case may be related to the porous nature of the support that favours a higher contact time between the reactive gas and the oxide.

A view of the morphological changes of CZ in the anode as a consequence of the redox treatment is given in Fig. 5. The micrographs taken at low (left side) and high resolution (right side) are related to samples a′, b′, c′. In sample a, CZ is distributed on the surface of YSZ pores of pellets forming aggregates of small particles and patches with a limited number of crakes. As the temperature of the reduction increases it is possible to observe an increment of crakes in the CZ film along with a coarsening and densification of

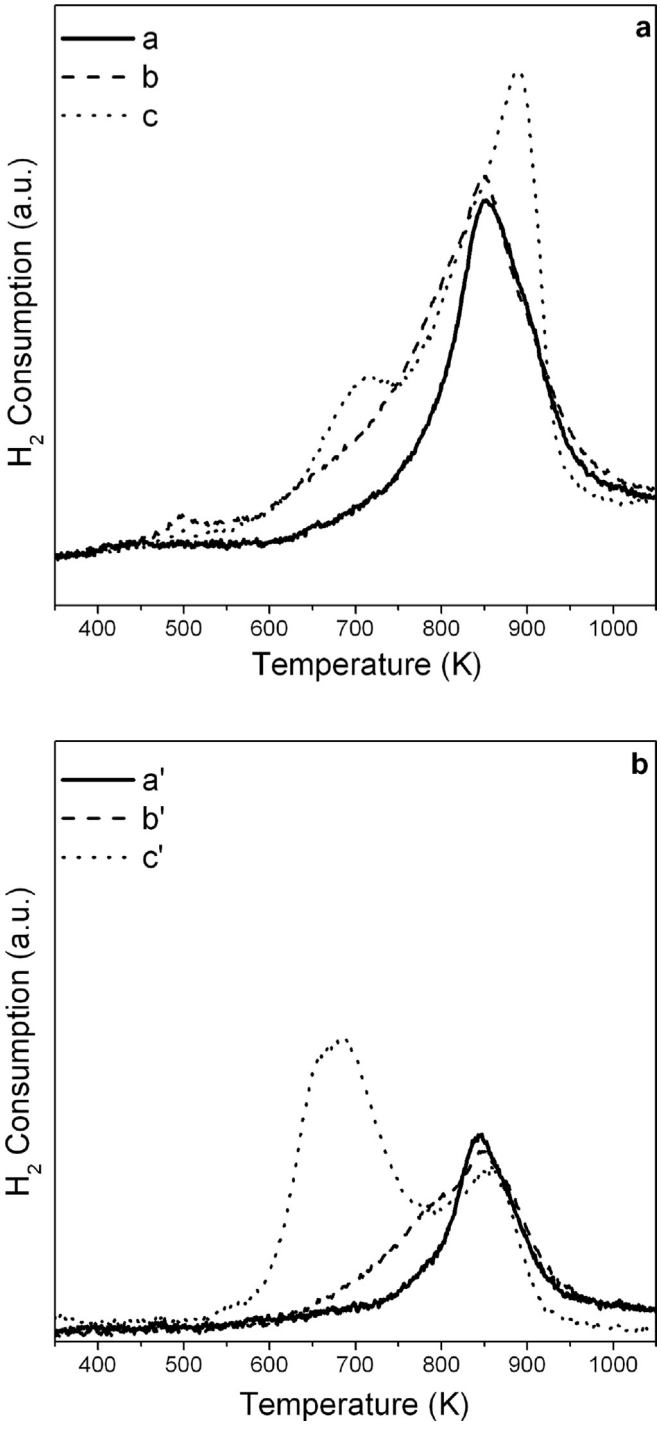

Fig. 4. a) TPR profiles of CZ powders: (—) a, CZ1073o; (---) b, CZ1073r; (···) c, CZ1273r. **b)** TPR profiles of porous pellets impregnated with CZ: (—) a′, CZ1073o/YSZ, (---) b′, CZ1073r/YSZ; (···) c′, CZ1273r/YSZ.

the CZ particles (b). In sample c, it is evident that the reduction at high temperature affects also the surface of YSZ backbone causing a sort of roughness. These microstructural modifications most probably occur also at electrolyte/electrode interface and may have consequence on performance of cells.

3.2. *Effect of the CZ structural changes on the performance of cells*

The electrochemical activity of Cu–CZ/YSZ||YSZ||LSM/YSZ cells having modified CZ catalysts is compared in Fig. 6. It was expected

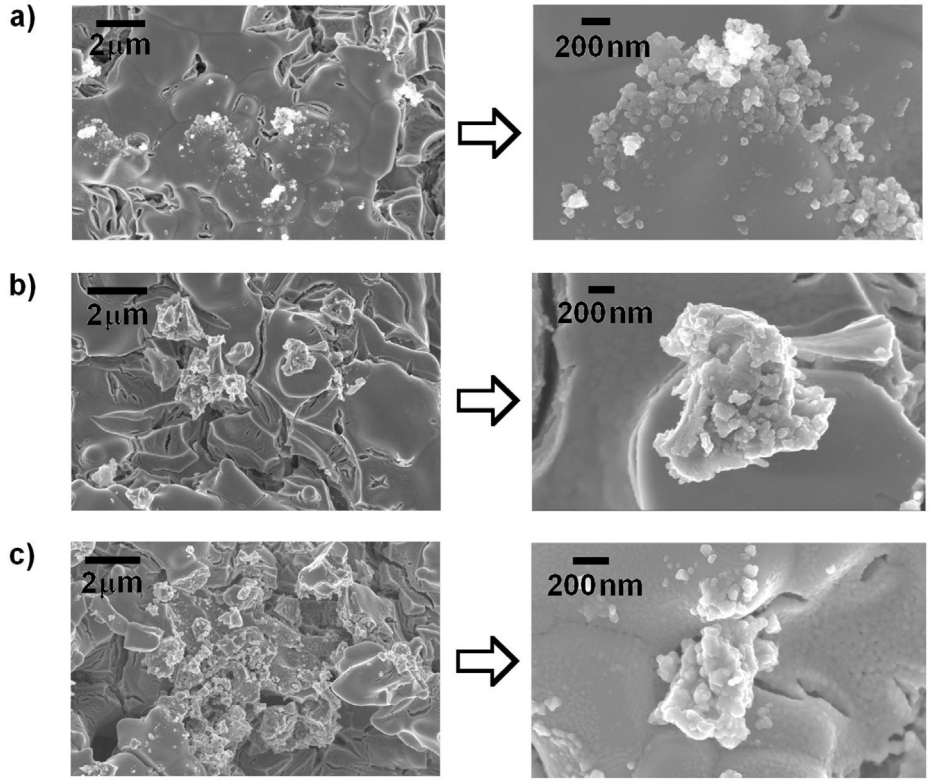

Fig. 5. SEM Micrographs of pellets impregnated with CZ and then calcined at 1073 K/4 h (a), reduced at 1073 K for 72 h (b), reduced at 1273 K for 24 h (c). At right high resolution images.

that the occurrence of enhanced phases with a higher reducibility and improved electronic conductivity would have increased cell performances. Conversely, Fig. 6a shows that the anodes which underwent strongly reducing ageing (B and C) showed lower performances than the untreated anode (A). This is partially due to the loss of surface area caused by the thermal and redox treatment. However, the decrease in power density of the treated samples is higher than the corresponding drop in surface area, this implies that other degradation phenomena occurred during the redox treatments.

Fig. 7 shows the corresponding Nyquist (a,b) and Bode plot (c,d) of the cells. The Nyquist plots of these cells (Fig. 7a) show two main arcs, one at high frequency (HF) (80–100 KHz) and one depressed arc at low frequency (LF) (10–15 Hz); a third process at intermediate frequency (400–1000 Hz) is sometime visible. Differences among the spectra were attributed to the anode characteristics since the cells were made and tested in the same way but the CZ catalyst underwent a different redox treatment. It is worth noting that for electrode A, the component at high frequency is almost negligible. In literature [34] the component at low frequency of CZ based anode is associated with dissociative adsorption and diffusion processes while the high frequency arc is related to charge transfer phenomena. It was demonstrated that charge transfer process is not the limiting step of reaction while chemical exchange process of oxygen containing species and bulk diffusion are limiting factors.

The cathode contribution to the total polarization should be of the same order for the three samples since cathode manufacture and size is the same for the three cells. Recent studies on an LSM/YSZ cathode prepared through infiltration reported value of polarization of 0.5 Ω cm^2 [64], which is much lower than what we measured. Thus, it is assumed that the relative cathode component is convoluted in the arcs at high-middle frequencies and it remains constant with respect the anode contributions. It is observed that for the samples that underwent redox treatments the first intersection of the spectrum with the Z′(R) axis moves at higher value and both the width and the apex of arcs increase. Specifically, the largest modification was observed for the component at high frequency (≈100 KHz). Thus, the reduction treatments negatively affect both the ohmic resistance and the total polarization of the cells. Table 2 reports the values related to the ohmic component R_Ω and to the cells' polarization R_{pol} (HF + LF components).

It is reported that an increase in polarization resistance with no corresponding changes in peak frequency and a simultaneous and proportional rise in series resistance, is a characteristics consequence of delamination [65]. In our case, the inference of a degradation due to delamination has been confirmed via a careful optical microscopy analysis of the electrolyte/electrode interface after the cell testing. Both the (B), and (C) electrodes showed interfacial areas no longer attached at the electrolyte, while the untreated electrode (A) remained well attached. This behaviour is consistent with the microstructural changes observed in Fig. 5. The development of mechanical strains during the redox process and the consequent delamination of the electrodes seem to be correlated to the intrinsic expansion of the CZ lattice when Ce^{4+}, which has a radius of 0.93 nm, is reduced to the larger Ce^{+3} ($r = 0.103$ nm) and to the coarsening of the catalysts. Moreover, at high temperature the strains associated with the redox process may be amplified by the structural changes of CZ (pyrochlore phase has a lattice parameter of 10.70 Å compared to a value of 5.08 Å for the fluorite structure). In addition, these materials show a behaviour more and more capacitive as the frequency increases, especially after redox treatments. In the range of the high frequencies an increase in the capacitance is generally attributable to an increase in the transfer charge resistance between electrolyte and electrode [66]. This is caused by a reduction of active sites at the interface due to the

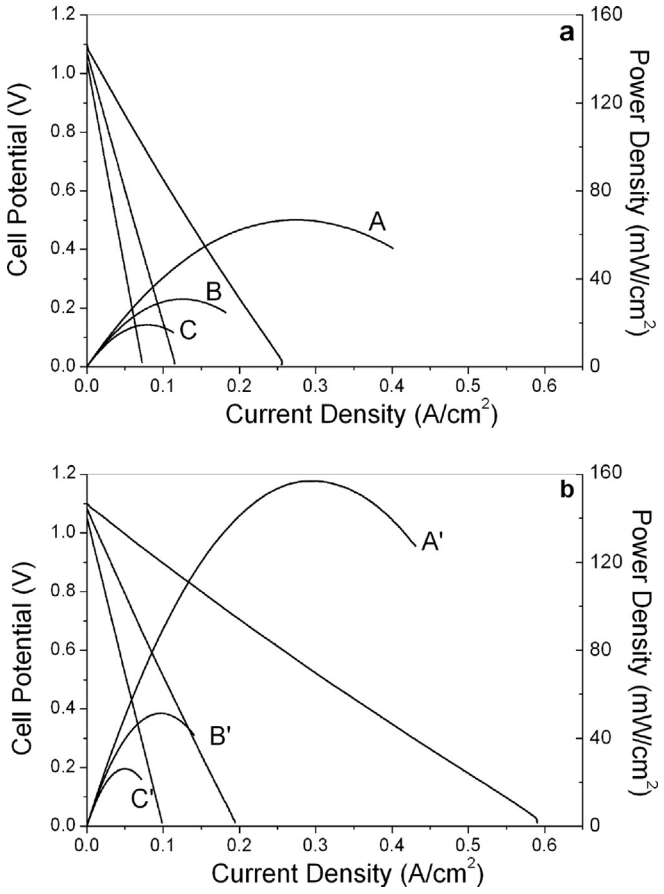

Fig. 6. a) *V–J* curves of single Cu–CZ/YSZ||YSZ||YSZ/LSM cells, anode impregnated with Cu and CZ which underwent different redox treatments: (A) electrode with CZ1073o, (B) electrode with CZ1073r, (C) electrode with CZ1273r, in 3% humidified H_2 flow, at 973 K. **b)** *V–J* curves of single Cu–CZ/YSZ||YSZ||YSZ/LSM cells as in Fig. 6a after an oxidation step at 973 K and subsequent reduction; (A′), (B′), (C′) respectively A, B, C after the redox cycle; in 3% humidified H_2 flow, at 973 K.

catalyst sintering, and to microstructural and morphological changes of electrolyte/electrode interface by the redox treatment.

Taking into account all the above observations, it is possible to conclude that redox treatments at temperatures over 1073 K, in the presence of CZ strongly impact the anode microstructure and in particular the interface, thus degrading the cell performance. Microstructural evolution of the anode and interface is linked to the mechanical stresses that develop as a result of the expansion and contraction of the CZ lattice during the redox cycles. In this view, the possible formation of pyrochlore phases, which undergo expansion even more significant, contributes negatively rather than positively to the cell performance. In addition, the electrolyte/electrode interface and the porous YSZ backbone could be subject to degradation processes due to the intrinsic mobility of the catalyst. In fact, it is reported that in redox conditions similar to those adopted in this study the cerium oxide in the form of film can epitaxially interact with the YSZ and undergo reconstruction processes of agglomeration and dispersion depending on the atmosphere of exposure [29].

The effect of a redox cycle on the full electrode Cu–CZ composition was investigated in situ through the oxidation and subsequent reduction of the anode at 973 K, after having kept it under H_2 for one day. Figs. 6b and 7b,d show respectively *V–J* curves and EIS spectra of the three anodes after the redox cycle (compare A, B, C with A′, B′, C′). Despite the type of CZ phases, all the cells showed enhanced performances in terms of power density due to a decrease of both the ohmic resistance and the cell polarization. The highest power density increment is observed for the untreated anode, almost 60%, while the other electrodes show an increase of 40% and 12% respectively. Referring to the EIS characterization, it is worth pointing out that the untreated electrode A shows significant changes such as the disappearance of the component at high frequency and the decrease of the arc at low frequency (10 Hz). The same effects, although in different proportions, are observed for the electrode B and C.

The most probable explanation for the common behaviour of these electrodes is that the redox treatment causes a redistribution of the active phases inside the YSZ porous matrix contributing to a higher compositional homogeneity between the CZ catalysts and the metallic electronic conducting phase [29,30]. On the other hand, the different increment observed in the three cells could be related to the different starting microstructure of the electrodes.

3.3. Characteristics of Cu–CZ/YSZ electrode before and after a redox cycle

3.3.1. Morphological and structural properties of Cu/YSZ and Cu–CZ50/YSZ electrodes

In order to clarify the origin of the enhancement of cells performance after the redox cycle, we focused on the morphological characterization of electrode A which showed the most significant EIS variation.

First, the morphology of single electrode components before and after redox treatment was investigated via SEM and HRTEM analysis. Fig. 8a and b show a map of 30 wt% Copper dispersion in a YSZ matrix before (a) and after (b) a redox cycle: after reduction at 973 K copper resulted segregated on the surface, an oxidation and subsequent re-reduction of the electrode led to a more homogeneous distributions of copper into the YSZ matrix and at the interface. SEM micrographs of CZ infiltrated into a porous YSZ layer show globules dispersed mainly at the electrolyte/electrode interface (results not shown) and looking down through HRTEM (Fig. 9a) it is possible to understand that the CZ globules are made of 5–12 nm crystallites. The Fourier transform (FT) image recorded for the YSZ support shows spots at 3.00 Å, which are ascribed to (101) crystallographic planes of tetragonal phase. The spots in the FT image recorded over the CZ crystallites at 3.10 Å correspond to (111) crystallographic planes and do not match the spatial positions of the YSZ spots, thus indicating that no structural relationship exists between the YSZ support and the CZ phase. Concerning details in the CZ structure, neither preferential facets are observed nor a pyrochlore phase is present. Fig. 9b shows that after the redox treatment the CZ crystallites suffered a morphological change. In fact, their sizes are wider than before the treatment and span from 3 to 20 nm, even in this case no particular preferred plane exposure was detected.

Secondly, the effects of redox cycles on reciprocal interactions between the active phases (Cu and CZ) into the porous YSZ layer were investigated and insight can be obtained from Fig. 10a and b. In each sample (before the redox treatment (a) and after (b)), a globular morphology is recognized for both YSZ and CZ. CZ globules of about 200–600 nm adhered well to the walls of the YSZ matrix while Cu is distributed over both YSZ and CZ. Moreover, CZ is always associated with Cu (no copper-free CZ globules were encountered in any case) indicating that Cu is dispersed over CZ, probably at a nanoscale level. By contrast, individual Cu particles are easily identified over YSZ. Cu particles over YSZ are round in shape, and their size being the only apparent difference in both samples. Before the redox treatment, Cu particles over YSZ are in the range 100–200 nm, after the redox cycle they are much smaller, about 10–50 nm in size.

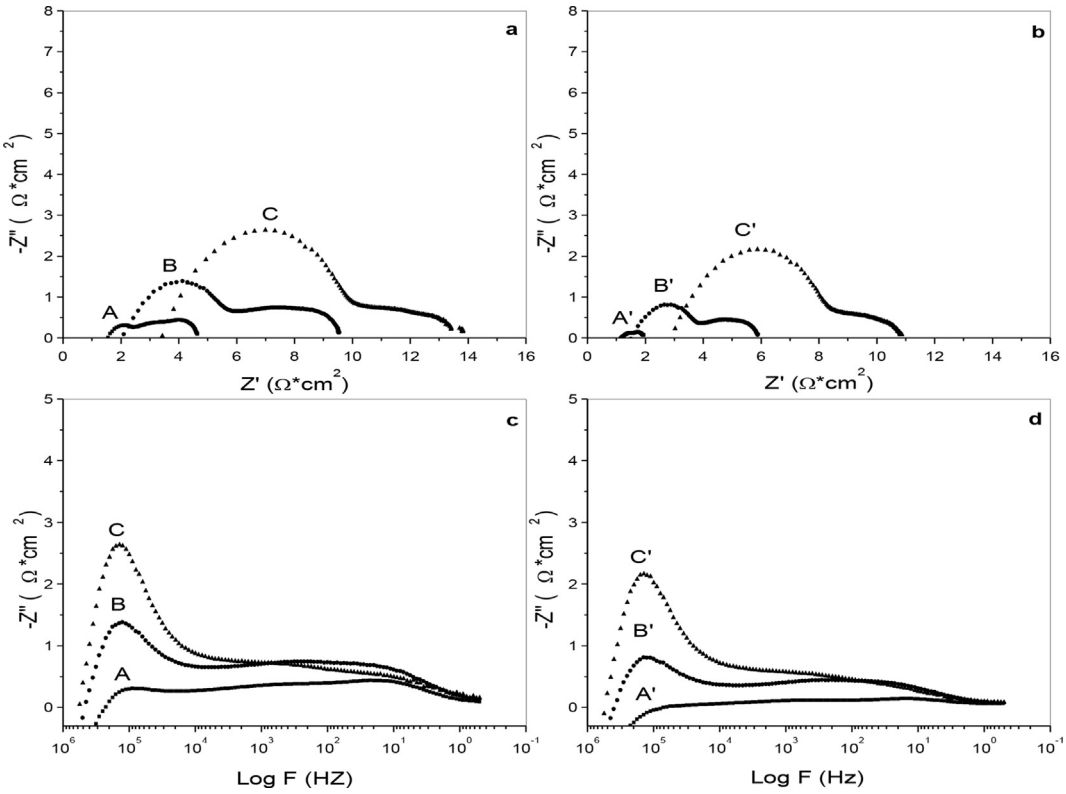

Fig. 7. a) Nyquist plots of single Cu–CZ/YSZ||YSZ||YSZ/LSM cells, anodes impregnated with Cu and CZ which underwent different redox treatments: (A) electrode with CZ1073o, (B) electrode with CZ1073r, (C) electrode with CZ1273r; in 3% humidified H_2 flow, at 973 K; bias 0 V **b)** Nyquist plots of single Cu–CZ/YSZ||YSZ||YSZ/LSM cells as in Fig. 7a after an oxidation step at 973 K and subsequent reduction; A′, B′, C′ respectively A, B, C after the redox cycle; in 3% humidified H_2 flow, at 973 K. **c)** Bode plot of a. **d)** Bode plot of b.

HRTEM images of the Cu–CZ/YSZ anode before and after the redox cycle are shown in Fig. 11a and b respectively. After reduction CZ particles are made of crystallites ranging from 5 to 15 nm, Cu crystallites are about 6–10 nm in size and it is evident that there is no epitaxial or structural relationship between YSZ support and CZ crystallites as well as no structural relationship between CZ and Cu crystallites. After the redox treatment (as occurred in the copper-free samples) it is possible to observe a disparity in sizes for CZ crystallites, which range from 5 to 30 nm. Moreover, Cu crystallites have clearly broken apart. Their sizes are about 4–6 nm, much smaller than those encountered in the only reduced sample. This is clearly shown in Fig. 11b where various Cu crystallites are labelled according to their lattice fringes, as well as several CZ particles. Further information comes from the inlet in which the FT image shows spots at 3.10 Å corresponding to (111) planes of CZ, which are not aligned with the spots at 2.09 Å of the (111) crystallographic planes of the Cu crystallite, demonstrating that no structural relationship exists between Cu and CZ crystallites.

To summarize, no structural and chemical interaction are evident among the components impregnated in the YSZ matrixes at least at the scale analyzed with SEM and HRTEM. The main effect of the low temperature redox cycle is a re-arrangement of CZ particle and a breaking apart of the copper crystallites. This causes a reorganization of copper and CZ morphology with a resulting increase in the surface area of the ionic conductor as well as an increase in connectivity and percolation of Cu through the YSZ matrix. Thus, an extension of the three phase boundary zone explains the enhanced performance of cells after the redox cycle. In the modified electrodes the redistribution of components are not able to overcome the interfacial damages caused by the severe treatments of reduction, and consequently the impact of redox treatment is less positive.

Table 2
EIS analysis at different temperatures, related to Cu–CZ/YSZ||YSZ||LSM/YSZ cells with CZ catalysts that underwent different redox treatments.

Temperature (K)	Type of anodes					
	Cu–CZ1073o/YSZ		Cu–CZ1073r/YSZ		Cu–CZ1273r/YSZ	
	R_Ω (Ω cm^2)	R_{pol} (Ω cm^2)	R_Ω (Ω cm^2)	R_{pol} (Ω cm^2)	R_Ω (Ω cm^2)	R_{pol} (Ω cm^2)
Before redox	(A)		(B)		(C)	
973	1.52	3.20	2.03	7.30	3.48	11.13
1023	1.32	1.73	1.59	4.17	2.36	5.62
1073	1.16	1.22	1.30	2.97	1.77	4.40
After redox	(A′)		(B′)		(C′)	
973	1.15	0.75	1.50	4.77	2.87	7.97
1023	0.96	0.50	1.25	2.87	2.04	4.98
1073	0.88	0.48	1.07	1.83	1.60	3.19

3.3.2. *Electrochemical properties of Cu/YSZ and Cu–CZ50/YSZ symmetrical cells*

Cu/YSZ and Cu–CZ/YSZ anodes in a symmetrical cell configuration were characterized with impedance spectroscopy in relation to their stability to time and redox cycles.

The Nyquist plot of the Cu/YSZ||YSZ||YSZ/Cu cell (Fig. 12) shows two main components at high and lower frequency. The ohmic resistance is higher than that expected for a 300 μm thick electrolyte [1], this suggests that the microstructure of porous electrodes contributes to ohmic resistance of the cell. The high ohmic resistance can be justified taking into account that in this study the microstructure of the electrodes is not optimized; the structure of the porous backbone consists of cluster not always well interconnected and the interface shows large cavities (see Fig. 1).

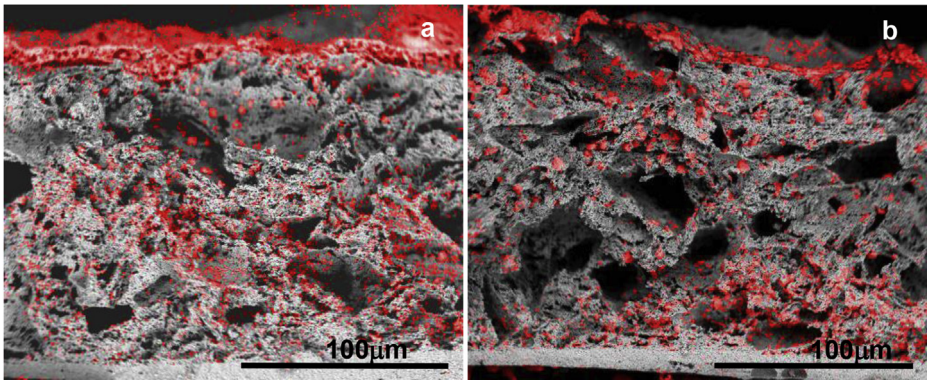

Fig. 8. SEM maps of 30 wt% copper dispersion (in red) in a YSZ porous matrix before (**a**), and after oxidation at 973 K and subsequent reduction (**b**). (For interpretation of the references to colour in this figure legend, the reader is referred to the web version of this article.)

The EIS spectrum of cell Cu–CZ/YSZ||YSZ||YSZ/CZ–Cu (Fig. 13) also shows two main components in the same range of frequencies, but ohmic and polarization resistance decrease significantly due to the addition of CZ that catalyses the electro-oxidation of H_2, and being a mixed ionic electronic conductors it may contribute to extend the three phase boundary. In the Cu/YSZ the low frequency component increases with time and this is attributed to a gradual copper segregation to the anode surface. The consequence of copper segregation is a less efficient conductive network, a decrease of three phase boundary, and possibly mass transport constrains due to surface pores plugging. It is worth noting that in this electrode the high frequency component shows negligible changes with the time, so as the ohmic resistance. Differently it is observed for the Cu–CZ/YSZ electrode (Fig. 13) where both the high and low frequency component increase with the time. The changes related to the high frequency arc suggest that with the time there is a modification of the interfacial zone, this is probably due to changes in the microstructure of the electrolyte/electrode interface and to a decrease of three phase boundary.

Other differences between the two electrodes are observed with respect to their behaviour in the redox cycles. After the redox treatment, polarization of the Cu/YSZ electrode decreased to a value close to the initial one, but slightly higher. Instead, polarization of the Cu–CZ/YSZ electrode dropped to a value much lower than that measured at the beginning, moreover repeated cycles allowed to keep it at a constant average (see inlet of Fig. 13). In this electrode an improvement of ohmic resistance was also observed. This would indicate the interactive role between CZ and Cu in the promotion of electrode activity. It is conceivable that the improvement in the electrochemical activity of this electrode after a redox cycle is related to changes in the number and in the nature of Cu–CZ interfaces. On the other hand, the improvement of ohmic resistance of Cu–CZ electrode implies a significant microstructural reconstruction of the electrode. This would improve the network between the components of the electrode favouring the percolation, and so the total conductivity of cell, moreover it would lead to a better interfacial contact with the electrolyte.

3.3.3. Redox properties of Cu/YSZ and Cu–CZ/YSZ electrodes

The redox properties of such Cu/CZ interfaces were investigated by means of temperature programmed reduction (TPR). The top of Fig. 14 shows the effect of redox treatment on TPR profiles of YSZ pellets impregnated with the cell anode composition (30% Cu and 10% CZ, 30Cu–10CZ/YSZ). For comparison, the bottom of Fig. 14 reports the TPR profiles of YSZ pellets impregnated with only CZ or CuO (Cu/YSZ, CZ/YSZ). The TPR profile of CZ shows an

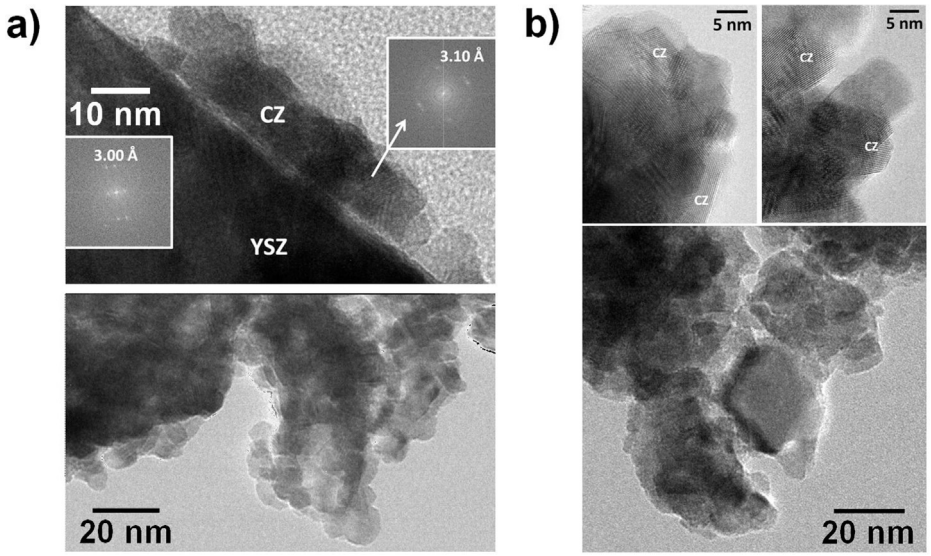

Fig. 9. HRTEM images of a YSZ matrix infiltrated with 10 wt% CZ before (**a**), and after oxidation at 973 K and subsequent reduction (**b**).

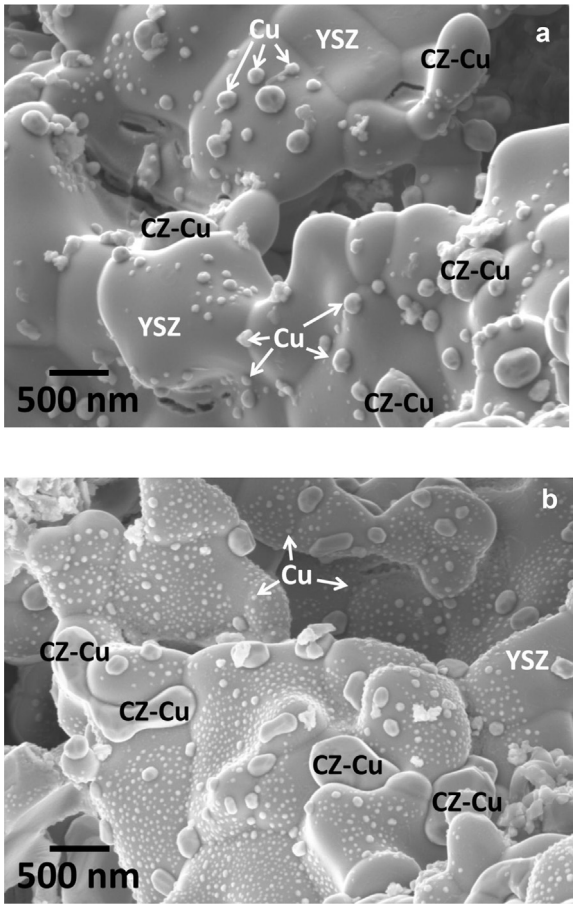

Fig. 10. SEM images of a YSZ slab infiltrated with both 20 wt% CZ and 10%Cu, before (**a**), and after oxidation at 973 K and subsequent reduction (**b**).

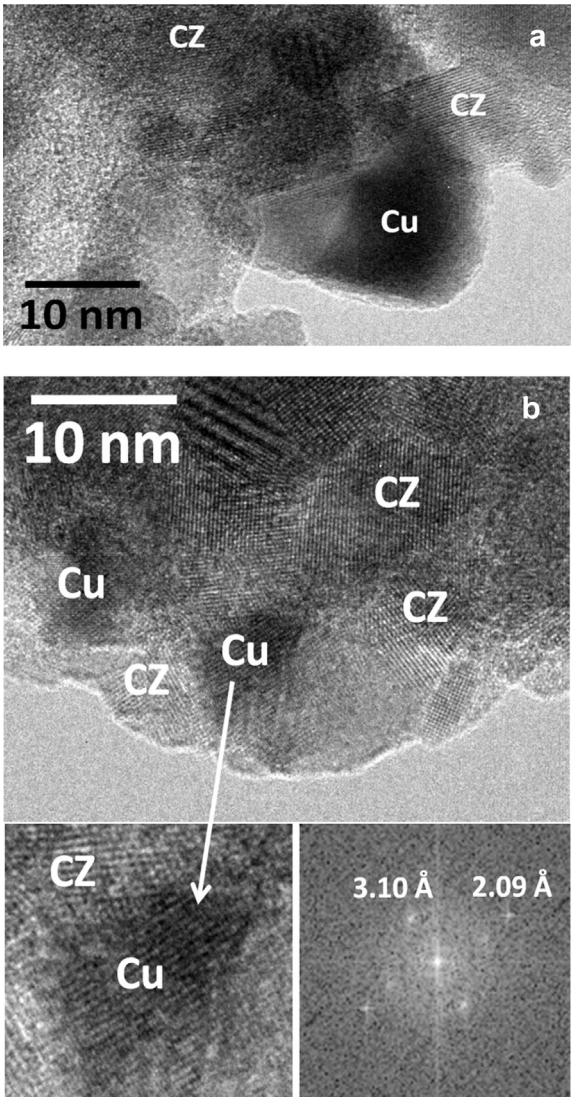

Fig. 11. HRTEM images of Cu–CZ/YSZ electrodes before (**a**), and after oxidation at 973 K and subsequent reduction (**b**).

asymmetric peak at 800 K and the reduction of Ce^{4+} to Ce^{3+} is complete, CuO reduces at much lower temperature and the corresponding TPR profile shows a multi peak with maxima at 520 K, 550 K and 570 K, even in this case the reduction is quantitative. The reduction of Cu–CZ composite leads to a complex TPR profile with two convolute peaks at 550 K and at 623 K and with a shoulder at 486 K. These observations are in agreement with the literature [67,68].

The sample (see top of Fig. 14) that underwent a redox treatment similar to the one adopted in testing the cells shows a slight shift of the profile at lower temperature showing a maximum at 520 K, moreover the component at higher temperature disappears. It is worthy to point out that quantitatively the degree of reduction is lower (76% rather 100% in the untreated sample). This behaviour could be consistent with the occurrence of a strong copper/cerium interaction that leave cerium reduced and copper oxidized. According to the literature, the formation of interfacial Cu–Ce oxides phases [69], characterized by the equilibrium $Ce^{4+} + Cu^{+} \leftrightarrow Ce^{3+} + Cu^{2+}$ favours the reduction of bulk ceria. In fact, this equilibrium causes a high concentration of oxygen vacancies, and the generation of an interface vacancies' gradient is the driving force in enabling high oxygen mobility into the ceria lattice. Moreover, these interfacial oxygen vacancies have been demonstrated to be good adsorbing sites for hydrogen adsorption, as well as for oxygen adsorption. Since pellets and electrodes have the same composition, we suppose that the same interaction between CZ and copper can assist the reduction mechanism at the level of the anode/electrolyte interface.

In the literature, it is reported that the contact strength between copper and ceria based supports is structure sensitive, and becomes stronger as the copper particle size decreases [70]. Since a lower copper loading favours its dispersion and in order to better

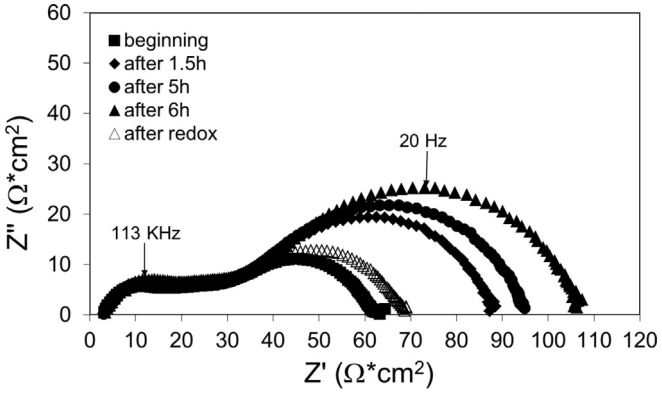

Fig. 12. Nyquist plots of a symmetrical Cu/YSZ||YSZ||YSZ/Cu cell with electrodes impregnated only with copper: response with the time and after oxidation at 973 K and subsequent reduction (after redox cycle), bias = 0.0 V, at 973 K, under dry H_2.

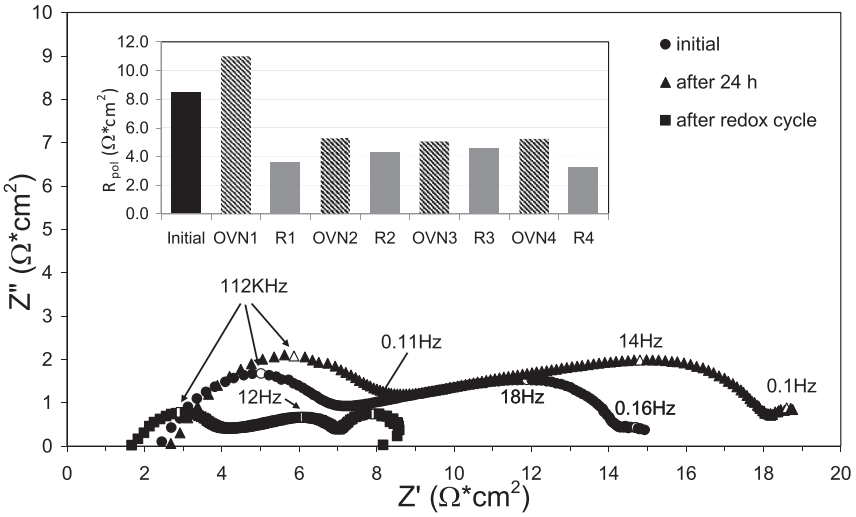

Fig. 13. Nyquist plots of a symmetrical Cu–CZ/YSZ||YSZ||YSZ/CZ-Cu cell with electrodes impregnated with copper and CZ: response with the time and after oxidation at 973 K and subsequent reduction (after redox cycle), bias = 0.0 V, at 973 K, under dry H_2. The inlet shows the cell polarization resistance in several days (OVNx = overnight) and after x repeated redox cycle (Rx).

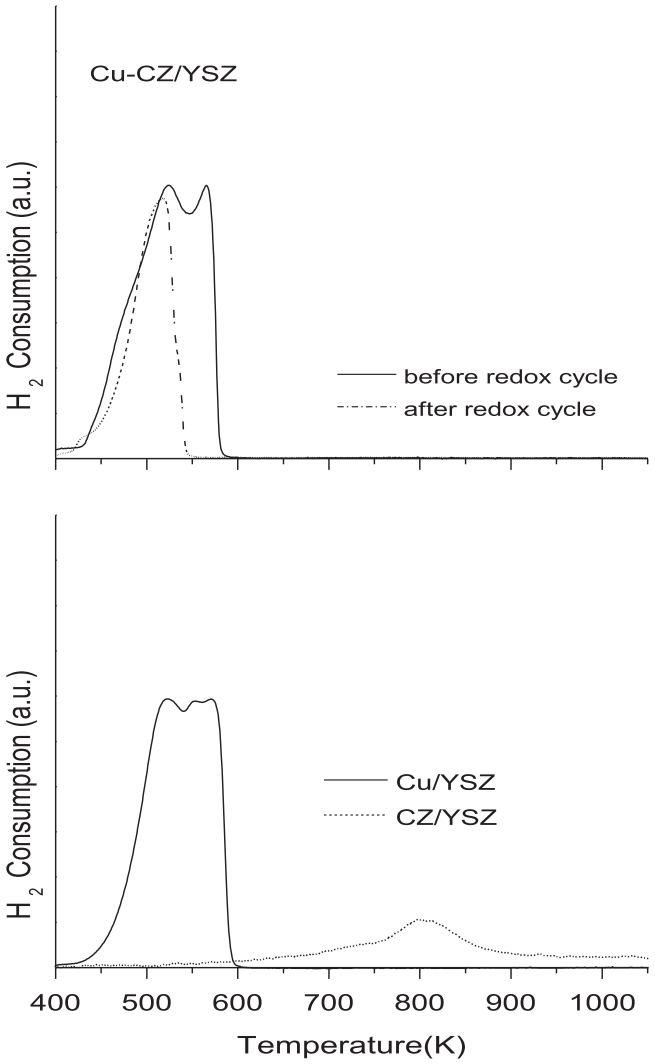

Fig. 14. TPR profiles of a YSZ pellet impregnated with 30 wt% Cu and 10 wt% CZ (Cu–CZ/YSZ) as infiltrated (before redox cycle) and after oxidation at 973 K and subsequent reduction (after redox cycle); TPR profiles of a YSZ pellet impregnated with 10 wt% CZ (CZ/YSZ) or 30 wt% Cu (Cu/YSZ).

appreciate the role of this parameter on the reducibility of the Cu/CZ interface, we carried out a double TPR measurement, which would simulate the redox treatment of the electrode, on a YSZ pellet loaded with a lower amount of copper (10 wt%).

Fig. 15 compares the TPR profiles of 10Cu–20CZ/YSZ pellets with those related to a pellet impregnated with only CuO (Cu/YSZ) and one impregnated with the anodic composition (30Cu–10CZ/YSZ). TPR profiles of all of the samples are complex traces constituting of two or three overlapped peaks. The intermediate component is attributable to the reduction of interfacial Cu–Ce oxides species in close contact with each other [67,70]. Instead, the peaks at the lowest and the highest temperatures are ascribable to highly dispersed copper species (i.e. two or three dimensional CuO nanoclusters or isolated copper ions) and to bulk-like CuO phases, respectively. In the samples with the CZ catalyst, the second TPR profiles show an increase in the peak component at intermediate temperature (520–530 K) and this is indeed evident for the sample loaded with a lower amount of Cu. Therefore, changes in TPR profile after the redox cycle are attributable to an increase in interfacial Cu–Ce oxides phases. It can be inferred that the same effect occurs when the electrode undergoes a redox treatment, thus justifying the TPR profiles in Fig. 14 (top) and higher electrochemical performance for the cells.

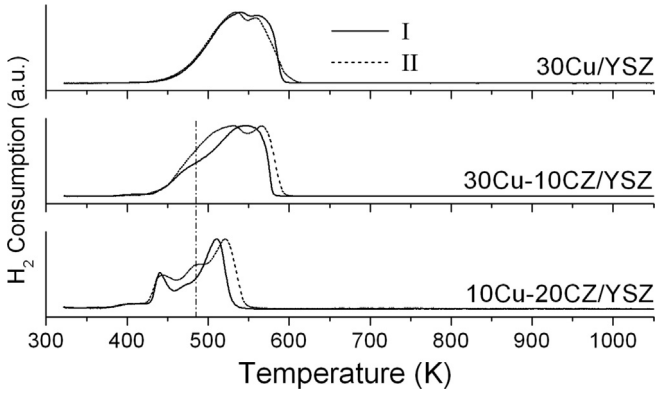

Fig. 15. Double TPR profiles of a porous pellet impregnated with 10 wt% Cu–20 wt% CZ (10Cu–20CZ/YSZ); with only 30 wt% Cu (30Cu/YSZ); and with the anodic composition 30 wt% Cu–10 wt% CZ (30Cu–10CZ/YSZ).

In short, to summarize this paragraph, the redox cycle is affective to favour a reconstruction of the Cu–CZ network mainly through copper re-dispertion, thus broadening the three phase boundary. As consequence of this re-dispersion copper and CZ nanoparticles also show a strong metal support interaction. The occurrence of an interfacial redox equilibrium between copper and CZ contributes to increase oxygen ion migration and the H_2 absorption, and consequently the kinetics of the electrode processes.

4. Conclusions

This study investigated the effect of redox properties of CZ on the performance of SOFC anodes prepared via infiltration of copper and CZ into YSZ porous layers.

Above 1073 K, under SOFC operating conditions the infiltrated CZ could undergo structural changes to pyrochlore phase. Despite the higher reducibility and electronic conductivity of the new phase, this structural modification would negatively affect the quality of electrolyte/anode interface of the cells causing delamination of the electrode. Conversely, at and below 1073 K structural changes would occur slowly and the main shortcoming would be a significant loss of surface area of the catalyst.

TPR, EIS and SEM characterizations confirmed that the interplay between copper and CZ has a fundamental role in determining the electrochemical activity of the electrode.

In situ redox cycles at 973 K caused the redistribution of anode components as well as a more intimate interaction between copper and CZ. This contributed to activate and to overcome the degradation of cell performance due to copper segregation.

To conclude, at intermediate temperature CZ is a suitable component to increase the redox and thermal resistance of Cu/Ce based anodes provided that an intimate contact between copper and CZ crystallites can be achieved. Further studies are in progress in order to gain insight in the nature of Cu–CZ interaction and to design anodes suitable for the most advanced IT-SOFCs applications.

Acknowledgements

Authors thank Prof. Fabrizio Cavani and their co-workers (University of Bologna) for the RAMAN characterization of powders, and the Italian Minister of the University and Research (MIUR) (cod. number 2010KHLKFC003) for funding the BIOITSOFC project (PRIN 2010), JL is grateful to ICREA Academia Program.

References

[1] S.C. Singhal, K. Kendal, High-temperature Solid Oxide Fuel Cells: Fundamentals, Design and Applications, first ed., Elsevier, Amsterdam, 2003.
[2] E.D. Wachsman, K.T. Lee, Science 334 (2011) 935–939.
[3] J.L. Brett, A. Atkinson, N.P. Brandon, S.J. Skinner, Chem. Soc. Rev. 37 (2008) 1568–1578.
[4] Y. Zhao, C. Xia, L. Jia, Z. Wang, H. Li, J. Yu, Y. Li, Int. J. Hydrogen Energy 38 (2013) 16498–16517.
[5] E.V. Tsipis, V.V. Kharton, J. Solid State Electrochem. 15 (2011) 1007–1040.
[6] W. Xiaodi, M. Ying, Z. Bin, Int. J. Hydrogen Energy 37 (2012) 19417–19425.
[7] M.C. Tucker, J. Power Sources 195 (2010) 4570–4582.
[8] Z. Liu, B. Liu, D. Ding, M. Liu, F. Chen, C. Xia, J. Power Sources 237 (2013) 243–259.
[9] H. He, Y. Huang, J. Regal, M. Boaro, J.M. Vohs, R.J. Gorte, J. Am. Ceram. Soc. 87 (2004) 331–336.
[10] A. Evans, A. Bieberle-Hütter, J.L.M. Rupp, L.J. Gauckler, J. Power Sources 194 (2009) 119–129.
[11] W. Wang, C. Su, Y. Wu, R. Ran, Z. Shao, Chem. Rev. 113 (2013) 8104–8159.
[12] R.J. Gorte, J.M. Vohs, Curr. Opin. Colloid Interface Sci. 14 (2009) 236–244.
[13] X.-M. Ge, S.-H. Chan, Q.-L. Liu, Q. Sun, Adv. Energy Mater. 2 (2012) 1156–1181.
[14] P.I. Cowing, C.T.G. Petit, R. Long, J.T.S. Irvine, S. Tao, Adv. Energy Mater. 1 (2011) 314–332.
[15] W.Z. Zhu, S.C. Deevi, Mater. Sci. Eng. A 362 (2003) 228–239.
[16] C. Chatzichristodoulou, P.T. Blennow, M. Sogaard, P.V. Hendriksen, M.B. Mogensen, in: A. Trovarelli, P. Fornasiero (Eds.), Catalysis by Ceria and Related Materials, Imperial College Press, London, (UK, 2013, pp. 623–758.
[17] E.P. Murray, T. Tsai, S.A. Barnett, Nature 400 (1999) 649–651.
[18] S. Park, J.M. Vohs, R.J. Gorte, Nature 404 (2000) 265–267.
[19] C. Gaudillère, P. Vernoux, C. Mirodatos, G. Caboche, D. Farrusseng, Catal. Today 157 (2010) 263–269.
[20] A. Jayakumar, A. Javadekar, J. Gissinger, J.M. Vohs, G.W. Huber, R.J. Gorte, AIChE J. 59 (2013) 3342–3348.
[21] A. Fuerte, R.X. Valenzuela, M.J. Escudero, L. Daza, J. Power Sources 196 (2011) 4324–4331.
[22] G. Bonura, C. Cannilla, F. Frusteri, Appl. Catal. B 121–122 (2012) 135–147.
[23] S.I. Lee, J.M. Vohs, R.J. Gorte, J. Electrochem. Soc. 151 (2004) A1319–A1323.
[24] K. Eguchi, T. Setoguchi, T. Inoue, H. Arai, Solid State Ionics 52 (1992) 165–172.
[25] A. Trovarelli, Comments Inorg. Chem. 20 (1999) 263–284.
[26] A.B. Kehoe, D.O. Scanlon, G.W. Watson, Chem. Mat. 23 (2011) 4464–4468.
[27] S. Zhao, R.J. Gorte, Appl. Catal. A 277 (2004) 129–136.
[28] S. Jung, C. Lu, H. He, K. Ahn, R.J. Gorte, J.M. Vohs, J. Power Sources 154 (2006) 42–50.
[29] O. Costa-Nunes, R.J. Gorte, J.M. Vohs, J. Mater. Chem. 15 (2005) 1520–1522.
[30] V. Perrichon, A. Laachir, S. Abouarnadasse, O. Touret, G. Blanchard, Appl. Catal. A 129 (1995) 69–82.
[31] H. He, J.M. Vohs, R.J. Gorte, J. Power Sources 144 (2005) 135–140.
[32] T. Kim, G. Liu, M. Boaro, S.-I. Lee, J.M. Vohs, R.J. Gorte, O.H. Al-Madhi, B.O. Dabbousi, J. Power Sources 155 (2006) 231–238.
[33] K. Ahn, H. He, J.M. Vohs, R.J. Gorte, Electrochem. Solid State Lett. 8 (2005) A414–A417.
[34] S. Song, R.O. Fuentes, R.T. Baker, J. Mater. Chem. 20 (2010) 9760–9769.
[35] M.G. Zimicz, P. Núñez, J.C. Ruiz-Morales, D.G. Lamas, S.A. Larrondo, J. Power Sources 238 (2013) 87–94.
[36] J.J. Delgrado, E. Del Rio, X. Chen, G. Blanco, J.M. Pintado, S. Bernal, J.J. Calvino, in: A. Trovarelli, P. Fornasiero (Eds.), Catalysis by Ceria and Related Materials, Imperial College Press, London, 2013, pp. 47–138.
[37] J. Kašpar, P. Fornasiero, in: A. Trovarelli (Ed.), Catalysis by Ceria and Related Materials, Imperial College Press, London, 2002, pp. 217–241,.
[38] T. Kim, J.M. Vohs, R.J. Gorte, Ind. Eng. Chem. Res. 45 (2006) 5561–5565.
[39] M. Boaro, A. Trovarelli, J.H. Hwang, T.O. Mason, Solid State Ionics 147 (2002) 85–95.
[40] G. Chiodelli, G. Flor, M. Scagliotti, Solid State Ionics 91 (1996) 109–121.
[41] J. Kaspar, P. Fornasiero, G. Balducci, R. Di Monte, N. Hickey, V. Sergo, Inorg. Chim. Acta 349 (2003) 217–226.
[42] J. Kearney, J.C. Hernandez-Reta, R.T. Baker, Catal. Today 180 (2012) 139–147.
[43] M.P. Yeste, C.J. Hernández, S. Bernal, G. Blanco, J.J. Calvino, J.A. Pérez-Omil, J.M. Pintado, Catal. Today 141 (2009) 409–414.
[44] M.P. Yeste, C.J. Hernández, S. Bernal, G. Blanco, J.J. Calvino, J.A. Pérez-Omil, J.M. Pintado, Chem. Mater. 18 (2006) 2750–2757.
[45] S. Bernal, G. Blanco, J.J. Calvino, J.C. Hernández, J.A. Pérez-Omil, J.M. Pintado, M.P. Yeste, J. Alloys Compd. 451 (2008) 521–525.
[46] Y.S. Christou, H. Bradshaw, C. Butler, J. Darab, A. Efstathiou, Top. Catal. 52 (2009) 2013–2018.
[47] R. di Monte, J. Kašpar, Catal. Today 100 (2005) 27–35.
[48] E. Aneggi, M. Boaro, C. de Leitenburg, G. Dolcetti, A. Trovarelli, J. Alloys Compd. 408 (2006) 1096–1102.
[49] M. Cimenti, J.M. Hill, Asia Pac. J. Chem. Eng. 4 (2009) 45–54.
[50] W. Wang, C. Su, T. Zheng, M. Liao, Z. Shao, Int. J. Hydrogen Energy 37 (2012) 8603–8612.
[51] D.H. Prasad, S.Y. Park, H. Ji, H.-R. Kim, J.-W. Son, B.-K. Kim, H.-W. Lee, J.-H. Lee, Appl. Catal. A 411–412 (2012) 160–169.
[52] M. Cimenti, J.M. Hill, J. Power Sources 195 (2010) 3996–4001.
[53] M. Liao, W. Wang, R. Ran, Z. Shao, J. Power Sources 196 (2011) 6177–6185.
[54] S. Song, M. Han, J. Zhang, H. Fan, J. Power Sources 233 (2013) 62–68.
[55] M. Boaro, S. Desinan, C. Abate, M. Ferluga, C. de Leitenburg, A. Trovarelli, J. Electrochem. Soc. 158 (2011) 22–29.
[56] T. Mahata, G. Das, R.K. Mishra, B.P. Sharma, J. Alloys Compd. 391 (2005) 129–135.
[57] A. Galenda, M.M. Natile, V. Krishnan, H. Bertagnolli, A. Glisenti, Chem. Mater. 19 (2007) 2796–2808.
[58] M. Boaro, J.M. Vohs, R.J. Gorte, J. Am. Ceram. Soc. 86 (2003) 395–400.
[59] S. Desinan, M. Boaro, C. Abate, M. Ferluga, C. de Leitenburg, A. Trovarelli, ECS Trans. 25 (2010) 335–344.
[60] H. Kishimoto, T. Omata, S. Otsuka-Yao-Matsuo, K. Ueda, H. Hosono, H. Kawazo, J. Alloys Compd. 312 (2000) 94–103.
[61] R.O. Fuentes, J.D. Woollins, R.T. Baker, J. Alloys Compd. 495 (2010) 565–569.
[62] H. Vidal, J. Kašpar, M. Pijolat, G. Colon, S. Bernal, A. Cordón, V. Perrichon, Appl. Catal. B 27 (2000) 49–63.
[63] T. Montini, N. Hickey, P. Fornasiero, M. Graziani, M.A. Bares, M.V. Martinez-Huerta, I. Alessandri, L.E. Depero, Chem. Mater. 17 (2005) 1157–1166.
[64] A. Torbi, A.R. Hanifi, T.H. Etsell, P. Sarkar, J. Electrochem. Soc. 159 (2012) B201–B210.
[65] L. Barelli, E. Barluzzi, G. Bidini, Int. J. Hydrogen Energy 38 (2013) 5060–5074.
[66] S.P. Jiang, S.P.S. Badwal, Solid State Ionics 123 (1999) 209–224.
[67] S.J. Gentry, N.W. Hurst, A. Jones, J. Chem. Soc. Faraday Trans. 1 77 (1981) 603–619.
[68] W.P. Dow, Y.-P. Wang, T.-J. Huang, Appl. Catal. A 190 (2000) 25–34.
[69] A. Łamacz, A. Krztòn, G. Djéga-Mariadassou, Catal. Today 176 (2011) 126–130.
[70] Lj Kundakovic, M. Flytzani-Stephanopoulos, Appl. Catal. A 171 (1998) 13–29.